Role of Tropical Clouds in Surface and Atmospheric Energy Budget

BAIJUN TIAN AND V. RAMANATHAN

Center for Atmospheric Sciences, Center for Clouds, Chemistry and Climate, Scripps Institution of Oceanography, University of California, San Diego, La Jolla, California

(Manuscript received 30 October 2000, in final form 6 August 2001)

ABSTRACT

In this paper diagnostic estimates of cloud radiative forcing (CRF) and clear-sky radiation budget at the surface and in the atmosphere, based on satellite-observed radiation budget at the top of the atmosphere (TOA) and empirical parameterizations derived from radiation models and field observations, are presented. This analysis is restricted to the tropical Pacific. High clouds over the intertropical convergence zone (ITCZ), the South Pacific convergence zone (SPCZ), and the warm pool (WP) exert a positive CRF of about 70 W m^{-2} within the atmosphere and a negative CRF of about -70 W m^{-2} at the surface, although with a negligible net CRF at the TOA. On the other hand, low clouds over the eastern subtropical Pacific and the equatorial cold tongue exert a negative CRF of about -20 W m^{-2} at the surface as well as in the atmosphere. The spatial gradients of the clear-sky radiation budget at the surface and in the atmosphere are small. In particular, it is shown that the clear-sky radiative cooling in the atmosphere is larger over the ITCZ, the SPCZ, and the WP, when compared with that over the subtropics and the cold tongue. Next, based on these diagnostic estimates and available surface turbulent heat flux data, the role of atmospheric CRF in the large-scale atmospheric moist static energy (MSE) transport is quantified. It is found that the atmospheric CRF provides the major energy source for balancing the divergence of MSE transport (from the ITCZ, the SPCZ, and the WP to the subtropics and the cold tongue) by the large-scale atmospheric circulation. On the other hand, the clear-sky radiative flux convergence and the surface turbulent heat fluxes have just the reverse spatial pattern and hence cannot satisfy the large-scale atmospheric MSE transport requirements.

1. Introduction

Clouds are shown to be one of the most important factors regulating the current climate system and future climate change (Ramanathan et al. 1989; Harrison et al. 1990; Cess et al. 1996). Thus measurements of cloud radiative forcing (CRF) at the top of the atmosphere (TOA), the surface, and in the atmosphere are essential to improve our understanding of earth's climate. With the advent of satellite observations, our knowledge of the CRF as well as clear-sky radiation budget at the TOA have improved substantially in the last few decades (Ramanathan et al. 1989; Harrison et al. 1990). However, little progress has been made in the climatologies of the CRF in the atmosphere and at the surface because of difficulties in accurately estimating clear-sky and cloud-sky radiation budget at the surface. Surface radiative fluxes have been measured (e.g., Cess et al. 1995; Collins et al. 1996; Waliser et al. 1996; Chou et al. 1998). However, due to the limited spatial distribution of surface radiometers and sampling problems inherent with point measurements, these observations lack enough spatial and temporal coverage and are less certain than the TOA satellite observations.

To fill that observational void, parameterizations have been developed by several research groups to calculate the surface radiative fluxes based on satellite-observed radiation fluxes at the TOA, and atmospheric and surface variables (e.g., Ramanathan 1986; Li and Leighton 1993; Stephens et al. 1994; Zhang et al. 1995; Gupta et al. 1999). The primary objective of this study is to present an improved diagnostic estimate of the atmospheric and surface CRF and the corresponding clear-sky radiation budget based on recent parameterizations derived from radiation models and field observations (Ramanathan and Collins 1991; Inamdar and Ramanathan 1994, 1997; Li et al. 1993b). We focus on the tropical Pacific (30°S–30°N, 120°–280°E) because of the availability of energy budget data and other correlative data from two field experiments conducted in the 1990s: The Tropical Ocean Global Atmosphere Coupled Ocean–Atmosphere Response Experiment (TOGA COARE) and the Central Equatorial Pacific Experiment (CEPEX). The timescale of this analysis is the climatological annual-mean averaged from 1985 to 1989. The present study differs from earlier studies in two respects: first, the procedures we employ for diagnosing surface

Corresponding author address: Baijun Tian, Center for Clouds, Chemistry and Climate, Scripps Institution of Oceanography, University of California, San Diego, 9500 Gilman Dr., La Jolla, CA 92093-0221.
E-mail: btian@ucsd.edu

radiation budget are drastically different, and thus provide an important new independent source for estimates of surface CRF and clear-sky radiative budget. Next, our analyses, as far as possible, take maximum advantage of the new data from TOGA COARE and CEPEX. Thus our estimates provide an important source for validation of general circulation model estimates.

Furthermore, the results presented in this study have important implications to the large-scale atmospheric moist static energy (MSE) transport, which are also described in detail. We combine available surface turbulent heat flux data with our improved estimates for the atmospheric and surface CRF and clear-sky radiation budget to investigate the role of the CRF in the surface heat budget and the large-scale atmospheric MSE transport. Several previous studies are relevant to this topic. Using *Nimbus-7* earth radiation budget data, Sohn and Smith (1992a,b) examined the role of clouds in the TOA energy budget and deduced their role in energy transport by the atmosphere–ocean system. They also showed that clouds diminished the differential heating between continents and oceans. Zhang and Rossow (1997) estimated the meridional energy transport by the atmospheric and oceanic general circulations relying on the radiative fluxes at the TOA. They derived the surface radiative fluxes employing cloud cover retrieved from the International Satellite Cloud Climatology Project (ISCCP) and characterized the effects of clouds on the zonal mean energy transports. They showed that clouds tend to reduce the requirements for the oceanic energy transport and enhance that for the atmospheric energy transport. However, the importance of the atmospheric CRF in the large-scale atmospheric MSE transport has not been fully explored by these earlier studies.

The plan for the rest of this paper is as follows: section 2 introduces data and analysis methods, while results and discussion are presented in section 3, followed by a summary of conclusions in section 4.

2. Data and analysis methods

The monthly mean data of clear-sky and cloudy-sky radiation flux at the TOA used in this study are from the Earth Radiation Budget Experiment (ERBE) for 1985–89. They consist of the clear-sky albedo, outgoing longwave (LW) radiation, and atmospheric greenhouse effect, as well as shortwave (SW) and LW CRF on a 2.5° × 2.5° grid. The ERBE data are capable of providing sufficient spatial, temporal, and diurnal sampling and accuracy of the radiation budget at the TOA.

The clear-sky net downward SW flux at the surface is taken from Li and Leighton (1993), which is a monthly mean dataset available for 1985–89. These data are produced using the ERBE data and a linear parameterization proposed by Li et al. (1993b), which relates the reflected SW flux at the TOA to the net SW flux at the surface in terms of only column water vapor amount and solar zenith angle. The test against available surface observations shows good agreement between the results of this parameterization and the surface observations (Li et al. 1993a).

The clear-sky downward LW flux at the surface (G_a^*) is estimated using Inamdar and Ramanathan's (1994, 1997) parameterization:

$$G_a^* = F_C\left(0.102\,68\,\ln w_{\text{tot}} + 0.034\,04 w_{\text{tot}} + 1.299\,22\frac{T_s}{300.0}\right) + 1.012\,766 G_a - 0.500\,65E, \quad (1)$$

where F_C and G_a are the clear-sky OLR and atmospheric greenhouse effect from ERBE data. Here E is the surface blackbody emission. T_S is the sea surface temperature (SST, in kelvins), taken from Reynolds (1988). The w_{tot} is the total column water vapor (g cm^{-2} or cm) estimated from special sensor microwave/imager data and the European Centre for Medium-Range Weather Forecasts data (Liu et al. 1992).

The fraction of CRF that contributes to the local heating of the atmosphere and the surface is quantified by f factors (Harshvardhan et al. 1990; Ramanathan and Collins 1991):

$$f_l = \frac{C_l(S)}{C_l(\text{TOA})} \quad (2)$$

$$f_s = \frac{C_s(S)}{C_s(\text{TOA})}, \quad (3)$$

where f_l and f_s are the LW and SW f factors for CRF. If the f factors were known, the CRF at the surface and in the atmosphere could then be computed based on ERBE data (Harshvardhan et al. 1990).

The LW f factor has different values for different cloud types. Clouds can be divided into three categories according to their cloud-top pressures p_c: high clouds, $p_c \leq 440$ mb; middle clouds, 440 mb $< p_c \leq 680$ mb; and low clouds, $p_c > 680$ mb (Hartmann et al. 1992). Figure 1 presents the climatological (11-yr average from July 1983 to June 1994) annual-mean cloud amounts for high and low clouds from ISCCP, while the climatological annual-mean LW CRF at the TOA from ERBE is shown in Fig. 2. In this study, we use the ISCCP cloud amount data to identify the geographical distribution of different cloud types.

High clouds, consisting of cirrus, cirrostratus, and deep convective clouds, are concentrated (over 25%) in the deep, moist convective regions, such as the intertropical convergence zone (ITCZ) and the South Pacific convergence zone (SPCZ) including the western Pacific warm pool (WP; Fig. 1a). These convective regions are mainly a result of high SSTs (>300 K) (e.g., Graham and Barnett 1987; Waliser and Graham 1993), which are also coincident with the ascending branches of the Hadley and Walker circulations. The cloud-top temper-

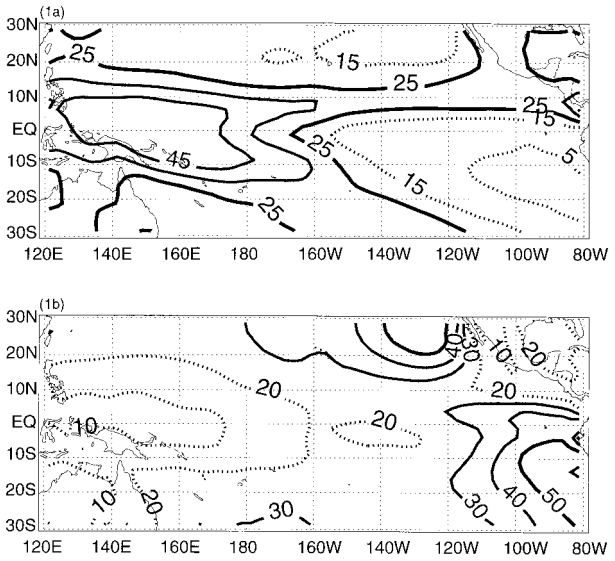

FIG. 1. The climatological (averaged from Jul 1983 to Jun 1994) annual-mean cloud amount from ISCCP: (a) high clouds ($p_c \leq 440$ mb), (b) low clouds ($p_c > 680$ mb). Unit: %.

atures of high clouds are much lower than the SSTs. Therefore, the LW CRF at the TOA due to high clouds is large, greater than 35 W m^{-2} (Fig. 2). The abundance of moisture in the atmosphere makes the atmosphere very strongly absorptive to LW radiation. As a result, downward LW fluxes due to high clouds are primarily absorbed by the moisture in the atmosphere and only marginally felt at the surface. Consequently, high clouds have a strong LW flux convergence in the atmosphere. In other words, the LW CRF due to high clouds is large in the atmosphere and small at the surface (e.g., Ramanathan 1987; Harshvardhan et al. 1990; Stephens et al. 1994; Webster 1994; Bergman and Hendon 1998, 2000; Sohn 1999; Chen et al. 2000). In order to estimate the value of f_l for high clouds, a modified form of the 20 cm^{-1} resolution LOWTRAN-7 (Kneizys et al. 1988) transmittance model is used to compute the LW CRF at the surface and the TOA in the WP (10°S–10°N, 120°–170°E). For the purpose of LW radiation, clouds can roughly be treated as a blackbody because of the near-unity emissivity. Thus all high clouds are assumed to be black, and the cloud top and thickness are specified as 11 and 3 km, respectively (f_l is not very sensitive to these specifications). The input temperature and humidity profiles for the radiative transfer calculations are soundings launched from ships from 1985 to 1989 (Inamdar and Ramanathan 1994). The results (Fig. 3a) indicate that f_l of high clouds lies between 0 and 0.25, with an average value of about 0.10, which is consistent with other studies based on radiation models and CEPEX observations (e.g., Ramanathan et al. 1995; Collins et al. 1996; Collins et al. 2000). For simplicity, we adopt 0.1 for f_l of high clouds in this study.

Low clouds are most predominant (over 30%) in the

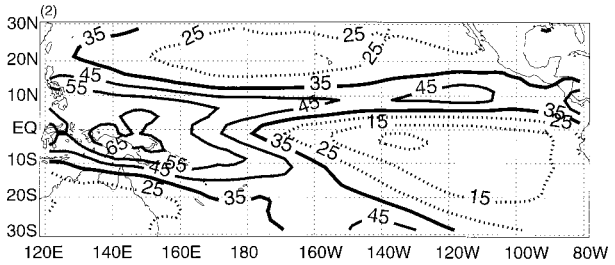

FIG. 2. The climatological (averaged over 1985–89, hereafter) annual-mean LW CRF at the TOA from ERBE. Unit: W m^{-2}.

cold oceans with lower than average SSTs (<298 K) such as the subtropics and the cold tongue, especially the subtropical eastern Pacific along the coasts of California and Peru, where the ocean upwelling is intense (Fig. 1b). Low clouds consist of stratus, stratocumulus, and cumulus clouds and are usually trapped below an inversion on the dry descending branches of the Hadley and Walker circulations. Because of their low cloud tops, the cloud-top temperatures are not much different from the SSTs. Therefore, LW CRF at the TOA due to low clouds appears to be minor, less than 25 W m^{-2} (Fig. 2). But, downward LW fluxes due to low clouds are substantial because of the warm cloud-base temperatures. Furthermore, since little moisture exists below the clouds, the downward LW fluxes are absorbed by the surface. Thus the LW CRF due to low clouds is

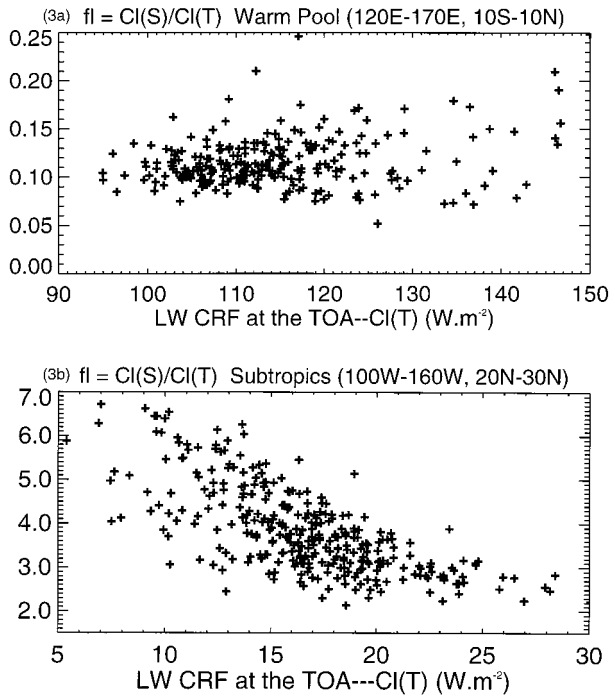

FIG. 3. The LW f factor for CRF base on a modified form of LOWTRAN-7. (a) High clouds in the western Pacific WP (10°S–10°N, 120°–170°E). (b) Low clouds in the subtropical northeastern Pacific (20°–30°N, 200°–260°E).

a strong energy source for the surface and much larger than that at the TOA. As a result, low clouds induce a net LW divergence in the atmosphere, resulting in a radiative cooling, especially of the lower troposphere (e.g., Harshvardhan et al. 1990; Nigam 1997; Bergman and Hendon 1998, 2000; Chen et al. 2000). Under these conditions, f_l of low clouds is greater than unity. To estimate the value of f_l for low clouds, the modified LOWTRAN-7 transmittance model is also used to compute the LW CRF at the surface and the TOA in the subtropical northeastern Pacific (20°–30°N, 200°–260°E). All low clouds are assumed to be black, and the cloud top and thickness are specified as 2.2 and 1.2 km, respectively. The results (Fig. 3b) indicate that f_l of low clouds is always greater than 2, but has strong variations between 2 and 7 (cf. Harshvardhan et al. 1990). For simplicity, we adopt 2.5 for f_l of low clouds in this study.

Middle clouds are much less common than high and low clouds in the Tropics and have no preferred regions (not shown). The LW CRF at the TOA due to middle clouds is roughly about 30 W m^{-2}, and their LW CRF at the surface has the same magnitude. Therefore, middle clouds have almost zero radiative effects in the atmosphere, that is, $f_l \approx 1$ (e.g., Chen et al. 2000). Of course an accurate estimation of LW CRF at the surface and in the atmosphere depends critically on the value of the f_l chosen; thus, the uncertainties of our results due to f_l is discussed in section 3d.

Clouds also have very complicated radiative effect on the atmosphere and the surface in the SW band. First, clouds shield the surface and the atmosphere below the clouds because of their high albedos, thereby decreasing the solar radiation absorbed at the surface and in the atmosphere by the water vapor below the clouds. Second, clouds increase the solar radiation absorbed in the cloud layer because they absorb more near-infrared radiation than water vapor and increase the average photon path length by scattering. Third, clouds also increase the upward SW flux at the cloud tops, consequently increasing the solar radiation absorbed by water vapor and ozone above the clouds. Many radiation model results suggest that irrespective of the optical depth or the cloud phase (water or ice cloud) or the cloud height, $f_s < 1.2$ (e.g., Ramanathan 1986; Harshvardhan et al. 1990; Li et al. 1993b). In other words, current radiation models suggest that clouds act merely to shade the sea surface from solar radiation with very little effect on the vertically integrated atmospheric solar absorption. But recent collocated satellite and surface measurements from TOGA COARE and CEPEX suggest that f_s is about 1.5 (e.g., Cess et al. 1995; Ramanathan et al. 1995; Pilewskie and Valero 1995). In other words, observations indicate that clouds also significantly enhance the vertically integrated atmospheric solar absorption. However, the issue of anomalous solar absorption by clouds has been a subject of intense debate (e.g., Chou et al. 1995; Arking et al. 1996; Li et al. 1997). For simplicity, we consider $f_s \approx 1.3$, which allows only a small amount of anomalous cloud absorption, but we also explore several different choices of f_s to examine the role of anomalous solar absorption in our results in section 3d.

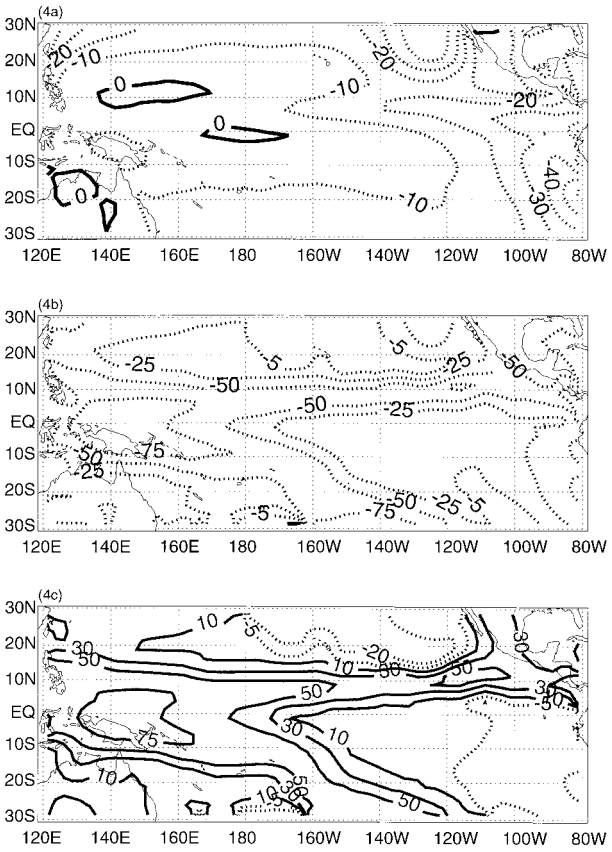

FIG. 4. The climatological CRF (a) at the TOA, (b) at the surface, and (c) in the atmosphere. Unit: W m^{-2}.

Direct measurements of surface turbulent heat fluxes are also very difficult and expensive, and few direct measurements are available. To overcome the lack of in situ measurements, bulk formulas have been developed to estimate surface turbulent heat fluxes from commonly observed fields such as surface air temperature, SST, dewpoint temperature, and wind speed. Using parameterizations, atlases of climatological global ocean surface turbulent heat fluxes have been developed (e.g., Oberhuber 1988; da Silva et al. 1994; Josey et al. 1999). The Oberhuber (1988), covering the period 1950–79, is the primary dataset for surface turbulent heat fluxes in this study because it has been used extensively.

3. Results and discussion

a. The CRF

Figure 4 shows the CRF at the TOA (Fig. 4a) from ERBE along with the present estimates of the CRF at the surface (Fig. 4b) and in the atmosphere (Fig. 4c). At the TOA, high clouds have both strong LW and SW

CRF because of high cloud tops and albedos, but the net CRF is negligible due to the strong compensation between the LW and SW CRF (e.g., Ramanathan and Collins 1991; Collins et al. 1996). On the other hand, low clouds have a strong radiative cooling effect because they have much higher albedos and yet their tops are not cold enough to have a large effect on the OLR (section 2). The importance of low clouds to the energy balance of the TOA can be demonstrated by a remarkable similarity between the distribution of the low-cloud amounts and the net TOA CRF (Klein and Hartmann 1993).

At the surface, the SW CRF due to low clouds is negative, while the LW CRF due to low clouds is positive (see section 2). The SW CRF is stronger than the LW CRF at the surface over the subtropical eastern Pacific along the coasts of California and Peru, where low clouds are predominant (Fig. 1b). Thus, low clouds have a net cooling effect of about -20 W m^{-2} at the surface. On the other hand, high clouds have a strong cooling effect at the surface due to the dominance of their SW CRF over their LW CRF. For example, the surface CRF is about -70 W m^{-2} in the ITCZ, the SPCZ, and the WP. Middle clouds seem to have a net cooling effect at the surface.

Within the atmosphere, high clouds have a strongly positive LW CRF, about 50 W m^{-2}, as well as a relatively large cloud solar absorption, about 10–20 W m^{-2}. Thus, the total CRF in the atmosphere due to high clouds is strongly positive, about 70 W m^{-2}, which is a strong energy source for the atmosphere. Thus high clouds have large competing effects on the atmospheric and the surface heat budget despite the small TOA effect. Within the atmosphere, low clouds have a strong LW cooling effect. The SW CRF in the atmosphere due to cloud solar absorption is very small. Consequently, the total CRF due to low clouds has a net radiative cooling effect on the atmosphere of about -20 W m^{-2}, which is a strong energy sink for the atmosphere. Middle clouds seem to have a slightly net warming effect within the atmosphere.

In summary, the CRF at the surface and in the atmosphere are largely controlled by different cloud systems. High clouds over the ITCZ, the SPCZ, and the WP exert a positive CRF of about 70 W m^{-2} within the atmosphere and a negative CRF of about -70 W m^{-2} at the surface although with a negligible net CRF at the TOA. On the other hand, low clouds over the subtropical eastern Pacific and the equatorial cold tongue exert a negative CRF of about -20 W m^{-2} at the surface as well as in the atmosphere.

b. The clear-sky radiation budget

Figures 5a and 6a show the clear-sky LW flux at the surface and into the atmosphere. At the surface, the LW flux has a net cooling effect, about 50–90 W m^{-2}. The minimum, about 50 W m^{-2}, is located in the WP. In the

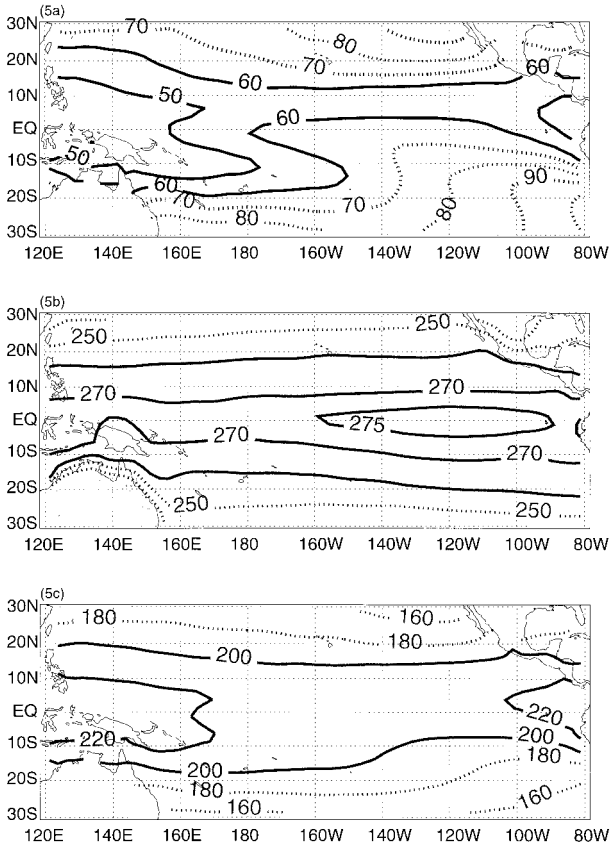

FIG. 5. The climatological annual-mean clear-sky radiative flux at the surface [$F_R^{\mathrm{clr}}(S)$]. (a) The LW flux calculated using ERBE data, and Inamdar and Ramanathan's (1994, 1997) parameterization. (b) The SW flux based on ERBE data, and the linear parameterization proposed by Li et al. (1993a). (c) Total. Unit: W m^{-2}.

atmosphere, the LW flux has a strong cooling effect throughout the Tropics due to the strong divergence of LW flux. The magnitude is around -200 to -240 W m^{-2}, comparable to the results in the empirical study of Stephens et al. (1994) and theoretical study of Sohn (1999). The minimum, about -240 W m^{-2}, is located in the ITCZ and the SPCZ, in particular the WP. The maximum, about -200 W m^{-2}, is located in the subtropics and the cold tongue. The spatial pattern of the clear-sky LW flux at the surface (into the atmosphere) closely follows the water vapor field and the SST pattern; in other words, the clear-sky LW flux at the surface (into the atmosphere) decreases with the increase of moisture, which in turn is a result of the increase of SST. This is consistent with the previous studies, such as Inamdar and Ramanathan (1994), Stephens et al. (1994) and Sohn (1999).

To further confirm the current result, which is based on a parameterization, the modified LOWTRAN-7 transmittance model is also used to compute the clear-sky LW heating in the WP (10°S–10°N, 120°–170°E) and in the subtropical northeastern Pacific (20°–30°N, 200°–260°E). The results (Fig. 7) show that the clear-

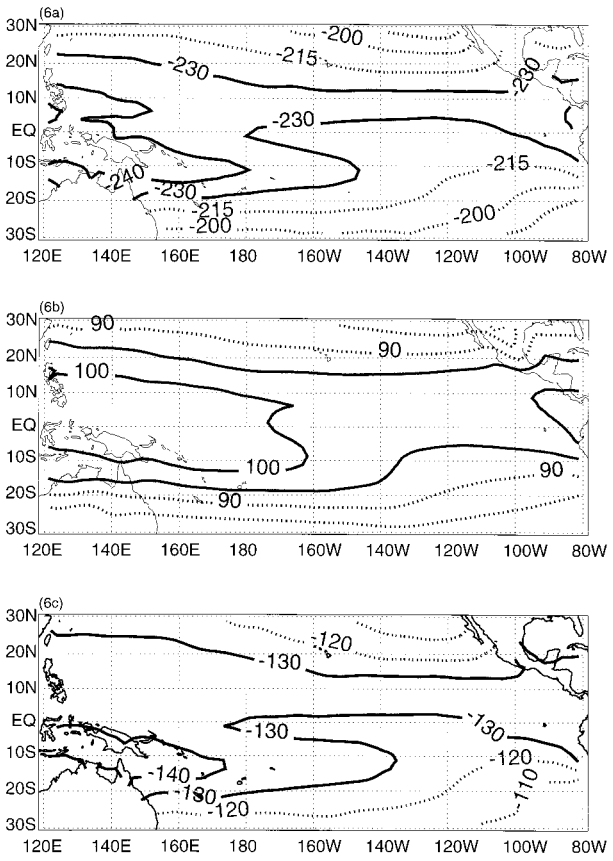

FIG. 6. The climatological annual-mean clear-sky radiative flux into the atmosphere [$F_R^{\text{clr}}(A) = F_R^{\text{clr}}(\text{TOA}) - F_R^{\text{clr}}(S)$] based on the clear-sky radiative flux at the TOA from ERBE and at the surface from Fig. 5. (a) LW, (b) SW, (c) total. Unit: W m^{-2}.

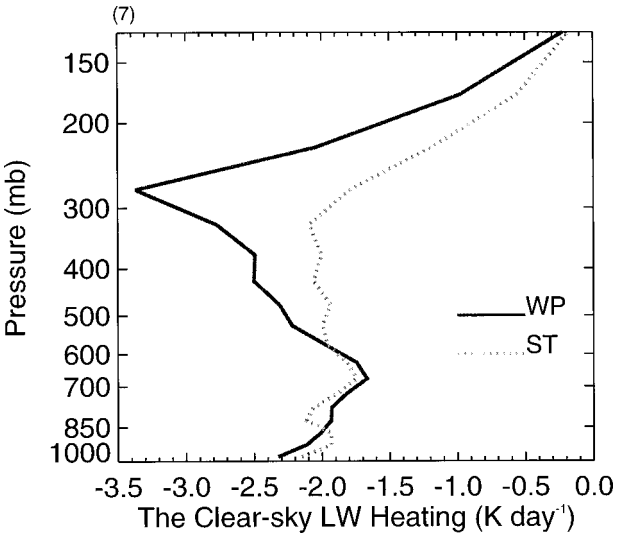

FIG. 7. The climatological annual-mean clear-sky LW radiative heating based on a modified form of LOWTRAN-7. The solid line is for the western Pacific WP (10°S–10°N, 120°–170°E), while the dotted line denotes the subtropical northeastern Pacific (20°–30°N, 200°–260°E).

sky LW cooling in the WP is stronger than that in the subtropics, which is consistent with our result based on the parameterization. The major difference between the WP and the subtropics is found in the upper troposphere above 600 mb, whereby the clear-sky radiative cooling in the WP is about 1 K day^{-1} stronger than that in the subtropics. This is consistent with the moisture profile, which shows that the strongest percent change in mixing ratio for the deep convective region from that of the nonconvective region is in the upper troposphere because of the deep convection (Inamdar and Ramanathan 1994). The lower-troposphere radiative cooling rate in the WP is almost the same as that in the subtropics. The possible reason for that is the following: the increase of moisture in the WP lower troposphere increases the lower-troposphere radiative cooling, while the increase of moisture in the WP upper troposphere decreases the lower-troposphere radiative cooling, through downward radiation. These two effects almost cancel each other.

The clear-sky SW radiation budget at the surface and in the atmosphere is shown in Fig. 5b and 6b. Not surprisingly, they are both positive. It is about 260 W m^{-2} at the surface due to the strong solar absorption by the surface and about 100 W m^{-2} in the atmosphere due to the strong solar absorption by water vapor. The patterns are more or less zonal with a small latitudinal gradient. The maxima are located at the equator and it decreases gradually poleward. It is apparent that these highly zonal patterns of atmospheric and surface solar absorption are due to the prime influences of the insolation at the TOA. Furthermore, the influence of the water vapor distribution is also very clear: the maximum of the atmospheric SW absorption by water vapor over the WP stands out in comparison with the lower-atmospheric SW absorption in the cold tongue.

Figures 5c and 6c show the clear-sky total radiative flux at the surface [$F_R^{\text{clr}}(S)$] and into the atmosphere [$F_R^{\text{clr}}(A)$]. At the surface, the clear-sky radiation flux has a net warming effect (about 200 W m^{-2}) due to the dominance of the SW radiation. On the other hand, because of the strong divergence of LW flux, $F_R^{\text{clr}}(A)$ is negative throughout the Tropics with the magnitude of around -100 and -140 W m^{-2} (e.g., Bergman and Hendon 2000). Comparisons of Fig. 5a with 5b and Fig. 6a with 6b show that the spatial gradients of the clear-sky solar absorption are much smaller than the LW flux, indicating that the spatial patterns of $F_R^{\text{clr}}(S)$ and $F_R^{\text{clr}}(A)$ are largely determined by the LW component. This is also revealed by the resemblance between the clear-sky LW and total radiative flux input (cf. Fig. 5a with 5c and Fig. 6a with 6c).

In summary, water vapor is the dominant regulator of the clear-sky total radiative flux at the surface [$F_R^{\text{clr}}(S)$] and into the atmosphere [$F_R^{\text{clr}}(A)$] mainly because of the downward LW emission to the surface. The $F_R^{\text{clr}}(S)$ is larger (stronger warming) around the equator and then decreases poleward. The $F_R^{\text{clr}}(A)$ is smaller (stronger

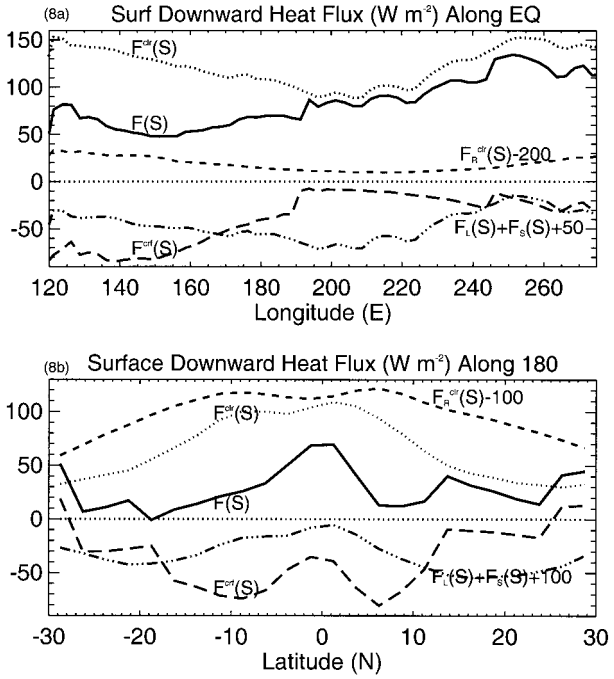

FIG. 8. The climatological annual-mean downward surface heat fluxes. (a) Zonal gradient along the equator. (b) Meridional gradient along 180°E. Unit: W m^{-2}.

cooling) in the ITCZ and the SPCZ than that in the subtropics and the cold tongue.

c. *Implications to the role of CRF in the large-scale atmospheric and oceanic energy transports*

For steady-state conditions, the energy conservation for the atmosphere and ocean system is

$$F(\mathrm{TOA}) = \nabla\cdot\mathbf{F}_A + \nabla\cdot\mathbf{F}_O, \tag{4}$$

where $F(TOA)$ is the net downward energy (i.e., radiative) flux at the TOA and $\nabla\cdot F_A$, $\nabla\cdot F_O$ denote the divergence of the large-scale atmospheric and oceanic energy transport.

For the surface only, we have

$$F(S) = \nabla\cdot\mathbf{F}_O, \tag{5}$$

where $F(S) = F_R^{\mathrm{clr}}(S) + F_R^{\mathrm{crf}}(S) - F_L(S) - F_S(S)$ is the net downward heat flux at the surface including clear-sky radiative flux [$F_R^{\mathrm{clr}}(S)$], surface CRF [$F_R^{\mathrm{crf}}(S)$], and latent and sensible heat fluxes (upward) [$F_L(S)$, $F_S(S)$]. We combine available surface turbulent heat flux data with our improved estimates of the surface CRF and clear-sky radiation budget to investigate the role of the CRF in the surface heat budget and the large-scale oceanic heat transport. The downward surface heat fluxes and their zonal cross section along the equator and the meridional cross section along 180° are shown in Fig. 8. Clearly, both the zonal and the meridional gradients of the cloudy-sky net downward heat flux at the surface, which balance the large-scale oceanic energy transport, are governed by the surface CRF. The clear-sky net downward heat flux into the ocean has a maximum in the WP, about 140 W m^{-2}, and decreases poleward to the subtropics. The clear-sky zonal gradient of the net downward surface heat flux between the WP and the cold tongue is negligible. However, when the CRF is included, the net downward surface heat flux in the WP is reduced to about 50 W m^{-2} because of the large negative SW CRF of high clouds. The reduced amount of the heat input into the ocean is transported into the atmosphere by convection through LW CRF and then exported into the subtropics and the cold tongue by the large-scale atmospheric circulation.

For the atmosphere only, the energy budget equation can be written as

$$F(A) = \nabla\cdot\mathbf{F}_A, \tag{6}$$

where $F(A) = F(TOA) - F(S) = F_R^{\mathrm{clr}}(A) + F_R^{\mathrm{crf}}(A) + F_L(S) + F_S(S)$ is the net energy flux into the atmosphere through the TOA and surface, which includes clear-sky radiative flux into the atmosphere [$F_R^{\mathrm{clr}}(A)$], atmospheric CRF [$F_R^{\mathrm{crf}}(A)$], and surface latent and sensible heat fluxes. Here $\nabla\cdot\mathbf{F}_A$ mainly presents the divergence of MSE transport by the large-scale atmospheric circulation (e.g., Tian et al. 2001). Many studies have shown that the atmospheric MSE transport is from the ITCZ and the SPCZ to the subtropics and the cold tongue (e.g., Oort and Peixoto 1983; Trenberth and Solomon 1994; Trenberth et al. 2001; Tian et al. 2001). In particular, the Hadley and Walker circulations are found to be the major MSE transport mechanism, while transient eddies seem to play a small role especially in the equatorial regions between 10°N and 10°S. Equation (6) states that the large-scale atmospheric circulation exports MSE ($\nabla\cdot\mathbf{F}_A > 0$) when the net energy flux input is positive ($F(A) > 0$) and vice versa. We will now compare the relative contribution of radiative and nonradiative (latent and sensible heat fluxes) to $F(A)$ to illustrate that the atmospheric CRF is the primary energy source that satisfies the spatial gradient requirements imposed by the atmospheric MSE transport.

Figure 9 presents the energy fluxes into the atmosphere and their zonal cross section along the equator and the meridional cross section along 180°. As discussed above, the spatial gradients of the clear-sky radiative flux into the atmosphere are small. In particular, it is shown that $F_R^{\mathrm{clr}}(A)$ is smaller (stronger cooling) in the ITCZ and the SPCZ than that in the subtropics and the cold tongue. Thus, the spatial gradients of the net energy flux into the atmosphere without the atmospheric CRF [$F^{\mathrm{clr}}(A)$] are mainly controlled by the surface turbulent heat flux, which is in turn determined by the surface latent heat flux. They both decrease from the subtropics to the equator. In the subtropics, weakly positive $F^{\mathrm{clr}}(A)$ is found because of the small clear-sky LW flux divergence and the large surface latent heat flux. In contrast, negative $F^{\mathrm{clr}}(A)$ dominates in the equatorial

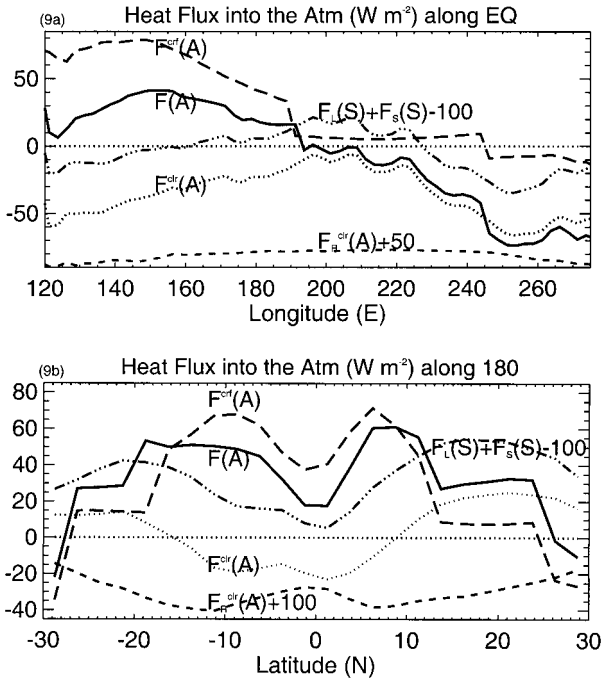

FIG. 9. The climatological annual-mean heat flux into the atmosphere. (a) Zonal gradient along the equator. (b) Meridional gradient along 180°E. Unit: W m^{-2}.

regions between 10°N and 10°S. The spatial gradient of $F^{\mathrm{clr}}(A)$, that is, positive in the subtropics and negative in the equatorial regions, is contrary to the required energy input by the large-scale atmospheric MSE transport (e.g., Oort and Peixoto 1983; Trenberth and Solomon 1994; Trenberth et al. 2001; Tian et al. 2001). Thus, in the present climate, neither the clear-sky radiative flux nor the turbulent heat fluxes have the appropriate spatial gradients to provide the balance for the divergence of the large-scale atmospheric MSE transport.

On the other hand, the different cloud systems between the deep convective and the subsidence regions induce a strong spatial gradient of energy source for the atmosphere, which is positive in the moist convective regions and negative in the dry subsidence regions. As a result, the net energy flux into the atmosphere [$F(A)$] has a strong spatial gradient. It is positive, about 40 W m^{-2}, in the WP, about -60 W m^{-2} in the cold tongue, and about ± 10 W m^{-2} in the subtropical Pacific. This gradient is consistent with the required energy input by the large-scale atmospheric MSE transport (e.g., Oort and Peixoto 1983; Trenberth and Solomon 1994; Trenberth et al. 2001; Tian et al. 2001). Clearly it is the atmospheric CRF that provides the appropriate spatial gradient to balance the divergence of the large-scale atmospheric MSE transport.

In summary, only the atmospheric CRF has the appropriate spatial gradients to balance the divergence of large-scale atmospheric MSE transport, while the clear-sky radiative flux and the surface turbulent heat fluxes have just the reverse spatial pattern and hence cannot satisfy the MSE transport requirements. Thus, the atmospheric CRF seems to be the primary energy source that satisfies the requirements imposed by the atmospheric MSE transport.

d. The uncertainties in the analyses

In this section, we choose the net energy flux into the atmosphere [$F(A)$] as an example to discuss the uncertainties in our analyses. Rieland and Raschke (1991) comprehensively estimated the errors in ERBE data. Average root-mean-square (rms) sampling errors due to diurnal sampling for net radiation are about 3.5 W m^{-2} for three satellites combined versus 11 W m^{-2} for one satellite. When other uncertainties from data inversion procedures are included, the final ERBE rms uncertainty estimates for net radiation are about 10 W m^{-2} (see Trenberth and Solomon 1994). Thus the main source of uncertainty for $F(A)$ comes from the surface radiative and turbulent heat fluxes. Gleckler and Weare (1997) have examined the sources of error in the surface latent and sensible heat fluxes of Oberhuber (1988). They found that the systematic errors in bulk formulas, especially the systematic uncertainties due to exchange coefficient and surface wind speed, are dominant in the uncertainties of the surface turbulent heat fluxes. The overall uncertainties are about 30 and 10 W m^{-2}, respectively, for the latent and sensible heat fluxes in the tropical Pacific.

The actual value of f_s is unknown because of a fundamental gap in our current knowledge of the atmospheric solar absorption. We do not know whether clouds significantly enhance or have no effects on the vertically integrated atmospheric solar absorption. But the possible range is 1.1–1.5 (Ramanathan et al. 1995). Thus the uncertainties of the atmospheric CRF and $F(A)$ due to f_s will be about $0.2 \times C_s$ (TOA), that is, about 15 W m^{-2} for high and low clouds, and less than 10 W m^{-2} for middle clouds. The accurate value of f_l is also unknown. But the possible ranges are as follows: f_l lies between 0 and 0.25 for high clouds (Fig. 3a; Collins et al. 2000), while f_l is probably between 2 and 7 for low clouds (Fig. 3b). Thus for high clouds the uncertainties of the CRF due to f_l are relatively small, less than 15 W m^{-2}. On the other hand, for low clouds the uncertainties of the CRF due to f_l might be very large, about 30–40 W m^{-2}. For middle clouds the uncertainties of the CRF due to f_l might be around 20 W m^{-2}.

If the possible magnitudes of f_s and f_l are considered to be the cause of the uncertainties of the atmospheric CRF, then it is uncertain by about 20 W m^{-2} in the WP, north subtropical Pacific, and the central equatorial Pacific and about 30–40 W m^{-2} in the eastern subtropics and cold tongue due to the simple f model. Despite the large uncertainties, they are usually less than or comparable to the uncertainties of the surface turbulent heat

fluxes discussed above. Thus the major uncertainties of $F(A)$ come from the surface turbulent heat fluxes and are around 40 W m^{-2}. Nonetheless, a conclusion drawn from this study, that atmospheric CRF is the only energy source that meets the requirements imposed by the divergence of the large-scale MSE transport, seems to be robust.

4. Summary and conclusions

In this paper we present our diagnostic estimates of CRF and clear-sky radiation budget at the surface and in the atmosphere based on satellite-observed radiation budget at the TOA and empirical parameterizations derived from radiation models. The empirical parameterizations used here are developed by Inamdar and Ramanathan (1994, 1997), Ramanathan and Collins (1991), and Li et al. (1993b) and have been validated with field observations. We focus on the tropical Pacific (30°S–30°N, 120°–280°E) because of the availability of energy budget data and other correlative data from TOGA COARE and CEPEX.

The CRF at the surface and in the atmosphere are controlled by different cloud systems. High clouds consisting of cirrus, cirrostratus, and deep convective clouds are concentrated in the ITCZ and the SPCZ including the western Pacific WP (Fig. 1a), where the underlying SSTs are high (>300 K). These cloud systems exert a positive CRF of about 70 W m^{-2} within the atmosphere and a negative CRF of about −70 W m^{-2} at the surface although with a negligible net CRF at the TOA. On the other hand, low clouds consisting of stratus, stratocumulus, and cumulus clouds, are most predominant in the colder oceans with lower than average SSTs such as the subtropics and the cold tongue, especially the subtropical eastern Pacific along the coasts of California and Peru, where the ocean upwelling is intense (Fig. 1b). Low clouds exert a negative CRF of about −20 W m^{-2} at the surface as well as in the atmosphere. Under clear skies, water vapor is the dominant regulator of the radiation budget at the surface and in the atmosphere mainly through the downward LW emission to the surface. The atmospheric water vapor concentration is higher in the ITCZ and the SPCZ and lower in the subtropics and the cold tongue. As a result, the net downward radiative flux at the surface is bigger (stronger warming) around the equator and then decreases poleward and the net radiative flux convergence into the atmosphere is smaller (stronger cooling) in the ITCZ and the SPCZ than that in the subtropics and the cold tongue.

Based on these diagnostic estimates of CRF and clear-sky radiation budget as well as available surface turbulent heat flux data, we deduce the role of the atmospheric CRF in the large-scale atmospheric MSE transport. It is found that the spatial gradient of the atmospheric CRF, which is positive in the deep convective regions and negative in the subsidence regions, is consistent with the large-scale atmospheric MSE transport from the convective regions to the subsidence regions. On the other hand, none of the other energy sources (clear-sky radiation or latent or sensible heat flux from the surface) has the appropriate spatial gradient to balance the divergence of the large-scale atmospheric MSE transport. Therefore, according to the estimates presented here, the atmospheric CRF seems to be the primary energy source that satisfies the energy requirements imposed by the meridional as well as the zonal MSE transport by the large-scale atmospheric circulation.

Acknowledgments. The authors wish to thank Dr. Anand Inamdar for his valuable help on the surface downward LW flux parameterization, ERBE data, ship data, and LOWTRAN-7 radiation model. Numerous valuable discussions with Dr. Eric Wilcox, Dr. Bill Conant, and help from Margaret Loken and Eric Wilcox on English writing are greatly appreciated. We also want to thank Dr. S. C. Sherwood and three anonymous reviewers for their helpful comments and constructive criticism on an earlier version of the manuscript, which led to significant improvement in the quality of this paper. The clear-sky surface SW flux of Li and Leighton (1993) is downloaded from Canada Center for Remote Sensing. The ISCCP cloud data are downloaded from the ISCCP Web site at GISS. The surface turbulent heat fluxes of Oberhuber (1988) are downloaded from IRI/LDEO climate data library. This research was supported by Grant NSF ATM9405024 to Center for Clouds, Chemistry and Climate (C^4) and is C^4 Rep. 246.

REFERENCES

Arking, A., M.-D. Chou, and W. L. Ridgway, 1996: On estimating the effect of clouds on atmospheric absorption based on flux observations above and below cloud level. *Geophys. Res. Lett.*, **23,** 829–832.

Bergman, J. W., and H. H. Hendon, 1998: Calculating monthly radiative fluxes and heating rates from monthly cloud observations. *J. Atmos. Sci.*, **55,** 3471–3491.

——, and ——, 2000: The impact of clouds on seasonal cycle of radiative heating over the Pacific. *J. Atmos. Sci.*, **57,** 545–566.

Cess, R. D., and Coauthors, 1995: Absorption of solar radiation by clouds: Observations versus models. *Science*, **267,** 496–499.

——, and Coauthors, 1996: Cloud feedback in atmospheric general circulation models: An update. *J. Geophys. Res.*, **101,** 12 791–12 794.

Chen, T., W. B. Rossow, and Y.-C. Zhang, 2000: Radiative effects of cloud-type variations. *J. Climate*, **13,** 264–286.

Chou, M.-D., A. Arking, J. Otterman, and W. L. Ridgway, 1995: The effect of clouds on atmospheric absorption of solar radiation. *Geophys. Res. Lett.*, **22,** 1885–1888.

——, W. Zhao, and S. H. Chou, 1998: Radiation budgets and cloud radiative forcing in the Pacific warm pool during TOGA COARE. *J. Geophys. Res.*, **103,** 16 967–16 977.

Collins, W. D., F. P. J. Valero, P. J. Flatau, D. Lubin, H. Grassl, and P. Pilewskie, 1996: Radiative effects of convection in the tropical Pacific. *J. Geophys. Res.*, **101,** 14 999–15 012.

——, A. Bucholtz, P. J. Flatau, D. Lubin, F. P. J. Valero, C. P. Weaver, and P. Pilewskie, 2000: Determination of surface heating by convective cloud systems in the central equatorial Pacific from

surface and satellite observations. *J. Geophys. Res.*, **105,** 14 807–14 821.

da Silva, A. M., C. C. Young, and S. Levitus, 1994: *Algorithms and Procedures*. Vol. 1, *Atlas of Marine Surface Data*, NOAA Atlas NESDIS 6, 83 pp.

Gleckler, P. J., and B. C. Weare, 1997: Uncertainties in global ocean surface heat flux climatologies derived from ship observations. *J. Climate*, **10,** 2764–2781.

Graham, N. E., and T. P. Barnett, 1987: Sea surface temperature, surface wind divergence, and convection over the tropical oceans. *Science*, **238,** 657–659.

Gupta, S. K., N. A. Ritchey, A. C. Wilber, C. H. Whitlock, G. G. Gibson, and P. W. Stackhouse Jr., 1999: A climatology of surface radiation budget derived from satellite data. *J. Climate*, **12,** 2691–2710.

Harrison, E. F., P. Minnis, B. R. Barkstrom, V. Ramanathan, R. D. Cess, and G. G. Gibson, 1990: Seasonal variation of cloud radiative forcing derived from the Earth Radiation Budget Experiment. *J. Geophys. Res.*, **95,** 18 687–18 703.

Harshvardhan, D. A. Randall, and D. A. Dazlich, 1990: Relationship between the longwave cloud radiative forcing at the surface and the top of the atmosphere. *J. Climate*, **3,** 1435–1443.

Hartmann, D. L., M. E. Ockert-Bell, and M. L. Michelsen, 1992: The effect of cloud type on earth's energy balance: Global analysis. *J. Climate*, **5,** 1281–1304.

Inamdar, A. K., and V. Ramanathan, 1994: Physics of greenhouse effect and convection in warm oceans. *J. Climate*, **7,** 715–731.

——, and ——, 1997: On monitoring the atmospheric greenhouse effect from space. *Tellus*, **49B,** 216–230.

Josey, S. A., E. C. Kent, and P. K. Taylor, 1999: New insights into the ocean heat budget closure problem from analysis of the SOC air–sea flux climatology. *J. Climate*, **12,** 2856–2880.

Klein, S. A., and D. L. Hartmann, 1993: The seasonal cycle of low stratiform clouds. *J. Climate*, **6,** 1587–1606.

Kneizys, F. X., and Coauthors, 1988: Users guide to Lowtran 7. Air Force Geophysics Laboratory Rep. AFGL-TR-88-0177, 137 pp.

Li, Z., and H. G. Leighton, 1993: Global climatologies of solar radiation budget at the surface and in the atmosphere from 5 years of ERBE data. *J. Geophys. Res.*, **98,** 4919–4930.

——, ——, and R. D. Cess, 1993a: Surface net solar radiation estimated from satellite measurements: Comparisons with tower observations. *J. Climate*, **6,** 1764–1772.

——, ——, K. Masuda, and T. Takashima, 1993b: Estimation of SW flux absorbed at the surface from TOA reflected flux. *J. Climate*, **6,** 317–330.

——, L. Moreau, and A. Arking, 1997: On solar energy disposition: A perspective from observation and modeling. *Bull. Amer. Meteor. Soc.*, **78,** 53–70.

Liu, W. T., W. Tang, and F. J. Wentz, 1992: Precipitable water and surface humidity over global ocean from Special Sensor Microwave Imager and ECMWF forecasts. *J. Geophys. Res.*, **97,** 2251–2264.

Nigam, S., 1997: The annual warm to cold phase transition in the eastern equatorial Pacific: Diagnosis of the role of stratus cloud-top cooling. *J. Climate*, **10,** 2447–2467.

Oberhuber, J. M., 1988: An atlas based on ''COADS'' dataset: The budgets of heat, buoyancy and turbulent kinetic energy at the surface of the global ocean. Max-Planck-Institute for Meteorology Rep. 15, 199 pp.

Oort, A. H., and J. P. Peixoto, 1983: Global angular momentum and energy balance requirements from observations. *Advances in Geophysics*, Vol. 25, Academic Press, 355–490.

Pilewskie, P., and F. P. J. Valero, 1995: Direct observations of excess solar absorption by clouds. *Science*, **267,** 1626–1629.

Ramanathan, V., 1986: Scientific use of surface radiation budget data for climate studies. *Surface Radiation Budget for Climate Application*, J. T. Suttles and G. Ohring, Eds., NASA Reference Publication 1169, 58–86.

——, 1987: The role of earth radiation budget studies in climate and general circulation research. *J. Geophys. Res.*, **92,** 4075–4095.

——, and W. Collins, 1991: Thermodynamic regulation of ocean warming by cirrus clouds deduced from observations of the 1987 El Niño. *Nature*, **351,** 27–32.

——, R. D. Cess, E. F. Harrison, P. Minnis, B. R. Barkstrom, E. Ahmad, and D. Hartmann, 1989: Cloud-radiative forcing and climate: Results from the Earth Radiation Budget Experiment. *Science*, **243,** 57–63.

——, B. Subasilar, G. Zhang, W. Conant, R. Cess, J. Kiehl, H. Grassl, and L. Shi, 1995: Warm pool heat budget and shortwave cloud forcing: A missing physics? *Science*, **267,** 499–503.

Reynolds, R. W., 1988: A real time global sea surface temperature analysis. *J. Climate*, **1,** 75–86.

Rieland, M., and E. Raschke, 1991: Diurnal variability of the earth radiation budget: Sampling requirements, time integration aspects and error estimates for the Earth Radiation Budget Experiment (ERBE). *Theor. Appl. Climatol.*, **44,** 9–24.

Sohn, B.-J., 1999: Cloud-induced infrared radiative heating and its implications for the large-scale tropical circulation. *J. Atmos. Sci.*, **56,** 2657–2672.

——, and E. A. Smith, 1992a: The significance of cloud-radiative forcing to the general circulation on climate time scales—A satellite interpretation. *J. Atmos. Sci.*, **49,** 845–860.

——, and ——, 1992b: Global energy transports and the influence of clouds on transport requirements—A satellite analysis. *J. Climate*, **5,** 717–734.

Stephens, G. L., A. Slingo, M. J. Webb, P. J. Minnett, P. H. Daum, L. Kleinman, I. Wittmeyer, and D. A. Randall, 1994: Observations of the earth's radiation budget in relation to atmospheric hydrology. 4: Atmospheric column radiative cooling over the world's oceans. *J. Geophys. Res.*, **99,** 18 585–18 604.

Tian, B., G. J. Zhang, and V. Ramanathan, 2001: Heat balance in the Pacific warm pool atmosphere during TOGA COARE and CEPEX. *J. Climate*, **14,** 1881–1894.

Trenberth, K. E., and A. Solomon, 1994: The global heat balance: Heat transport in the atmosphere and ocean. *Climate Dyn.*, **10,** 107–134.

——, J. M. Caron, and D. P. Stepaniak, 2001: The atmospheric energy budget and implications for surface fluxes and ocean heat transports. *Climate Dyn.*, **17,** 259–276.

Waliser, D. E., and N. E. Graham, 1993: Convective cloud systems and warm-pool sea surface temperatures: Coupled interactions and self-regulation. *J. Geophys. Res.*, **98,** 12 881–12 893.

——, W. D. Collins, and S. P. Anderson, 1996: An estimate of the surface shortwave cloud forcing over the western Pacific during TOGA COARE. *Geophys. Res. Lett.*, **23,** 519–522.

Webster, P. T., 1994: The role of hydrological processes in ocean–atmosphere interactions. *Rev. Geophys.*, **32,** 427–476.

Zhang, Y.-C., and W. B. Rossow, 1997: Estimating meridional energy transports by the atmospheric and oceanic general circulations using boundary fluxes. *J. Climate*, **10,** 2358–2373.

——, ——, and A. A. Lacis, 1995: Calculation of surface and top of atmosphere radiative fluxes from physical quantities based on ISCCP data sets. 1: Method and sensitivity to input data uncertainties. *J. Geophys. Res.*, **100,** 1149–1165.